We are Nitinol.™

TiNi Oxidation: Kinetics and Phase Transformations

A.R. Pelton, A. Mehta, L. Zhu, C. Trépanier, V. Imbeni, S. Robertson, M. Barney, and A. Minor,

2005

TiNi OXIDATION:
KINETICS AND PHASE TRANSFORMATIONS

A. R. Pelton[1], A. Mehta[2], L. Zhu[1], C. Trépanier[1],
V. Imbeni[3], S. Robertson[4], M. Barney[4], and A. Minor[5]

[1]NDC, 47533 Westinghouse Dr., Fremont, CA 94539, USA
[2]SSRL/SLAC, Bldg. 137, MS 69, 2575 Sand Hill Road, Menlo Park, CA 94025, USA
[3]SRI International, 333 Ravenswood Ave. Menlo Park, CA 94025, USA
[4]Dept. of Materials Science and Engineering, U.C. Berkeley, Berkeley, CA 94720, USA
[5]National Center for Electron Microscopy, LBNL, Berkeley, CA 94720, USA

Keywords: oxidation, TiNi, TiO_2, Ni, Ni_3Ti

Abstract

This study explores the kinetics and phase transformations of $Ti_{49.2}Ni_{50.8}$ wires that were oxidized in air between 400 and 1000°C for 3 to 300 minutes. High spatial and angular analytical techniques such as SEM, FIB, and synchrotron microdiffraction, were used to characterize the thickness, composition, and phase distribution of the resultant surface layers. Oxidation was determined to follow a logarithmic rate with an activation energy of 22 kJ/mole in the 400°C to 600°C range. At 600°C-1000°C, oxidation follows a parabolic growth rate with an activation energy of 203 kJ/mol. The results of this study suggest that oxidation at higher temperatures occurs as follows:

$$4\,NiTi + 3O_2 \rightarrow Ni_3Ti + Ni + 3TiO_2$$
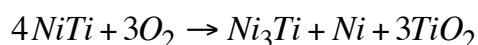
Introduction

Equiatomic Titanium-Nickel (TiNi or Nitinol) is an intermetallic compound characterized by a unique combination of properties, including thermoelasticity, corrosion resistance, and biocompatibility. These properties make it very attractive for biomedical applications, such as orthodontic archwires, minimally-invasive instrumentation, and self-expanding stents [1]. Thermoelasticity is manifested by thermal shape memory and mechanical superelasticity due to a well-documented reversible martensitic transformation [2]. Furthermore, investigators demonstrated that after appropriate passivation, TiNi surface consists mainly of a titanium-oxide (TiO_2) layer similar to that found on Ti alloys [4] with comparable *in vivo* biocompatibility [3]. However, recent studies concluded that thermal oxidation of TiNi can lead to surprisingly poor corrosion resistance [3,5]. As such, this paper reports on a systematic investigation of the kinetics and precipitation due to thermal oxidation of medical-grade Nitinol at high spatial and angular resolution.

Experimental Methods and Techniques

Material and Sample Preparation
Three-mm diameter $Ti_{49.2}Ni_{50.8}$ medical-grade wire was annealed at 1000°C for 30 minutes, centerless ground to remove the resultant oxide scale, and electropolished. Sections of the electropolished wire were subsequently oxidized in air between 400-1000°C in 100°C increments for 3, 10, 30, 100, and 300 minutes to simulate processing conditions.

Surface Analysis
Transverse and longitudinal wire samples were mechanically polished to 1200 grit SiC for metallographic examination; samples were not etched in order to preserve all phases for analysis. The thickness and composition of the oxide layers of these samples were characterized by various microstructural and spectrographic techniques. Auger Electron Spectroscopy (AES) and X-ray Photon Spectroscopy (XPS) depth profiles were used to characterize the wire surfaces with oxide thicknesses up to 100nm. Scanning electron microscopy (SEM) with high-resolution Focused Ion Beam (FIB) was used for oxide thicknesses ≥ 100nm. Conventional SEM was also used to characterize oxide thickness layers ≥ 1µm. SEM and FIB analyses were conducted primarily in backscattered-electron-imaging (BEI) mode to differentiate Ni- and Ti-rich phases. Structural phases were identified based on the analysis of powder diffraction patterns obtained with monochromatic x-ray beam (8keV) of spot size 2 x 7µm at synchrotron microdiffraction beamline 7.3.3 at the Advanced Light Source (ALS) at the LBNL [6].

Table 1: Oxide thickness as a function of temperature and time with analytical technique*. The initial oxide thickness of 11nm was measured by AES.

Time (min.)	Temperature (°C)						
	400	500	600	700	800	900	1000
	Oxide Thickness (µm)						
3	0.0200 A	0.0188 F	0.0338 F	0.119 A	2.737 S	6.052 S	11.23 S
10	0.0338 F	0.0244 F	0.0808 F	0.550 F	5.775 S	11.40 S	21.90 S
30	0.0282 F	0.0676 F	0.549 F	0.738 S	13.70 S	14.70 S	54.80 S
100	0.0470 F	0.0708 F	1.350 F	2.230 S	15.33 S	23.50 S	157 S
300	0.0670 F	0.0714 F	2.650 S	6.780 S	20.92 S	43.80 S	278 S

*Primary Analytical Technique: **A** = AES, **F** = FIB, and **S** = SEM

Results and Discussion

Oxidation Kinetics
Table 1 summarizes the resultant oxide layer thickness as well as the analytical techniques. These data plotted in Figure 1a illustrate the effects of time and temperature on oxide thickness. Note that there is an initial high growth rate followed by slower growth kinetics at each temperature. These data also demonstrate the expected trend of thicker oxides at higher temperatures. The 400-600°C data fit a logarithmic growth rate, whereas the 600-1000°C data fit better with a parabolic rate. These data are plotted per an Arrhenius relationship as shown in Figure 1b. An activation energy of 22 kJ/mol was determined for the low-temperature data and 203 kJ/mol for the higher temperatures.

Chu, *et al.* [7] obtained an activation energy of 226 kJ/mol (700-1000°C), and Chuprina [8] observed 180 kcal/mol (600-800°C) to 300 kcal/mol (800-1000°C). In comparison, titanium oxidizes with logarithmic kinetics (200-400°C) and transitions to a cubic fit (400-600°C). Parabolic growth (600-1000°C) is observed with an activation energy of 214 kcal/mol, which is comparable to the activation energy of diffusion of oxygen (250-300 kJ/mol) and titanium (330 kJ/mol) in rutile [4].
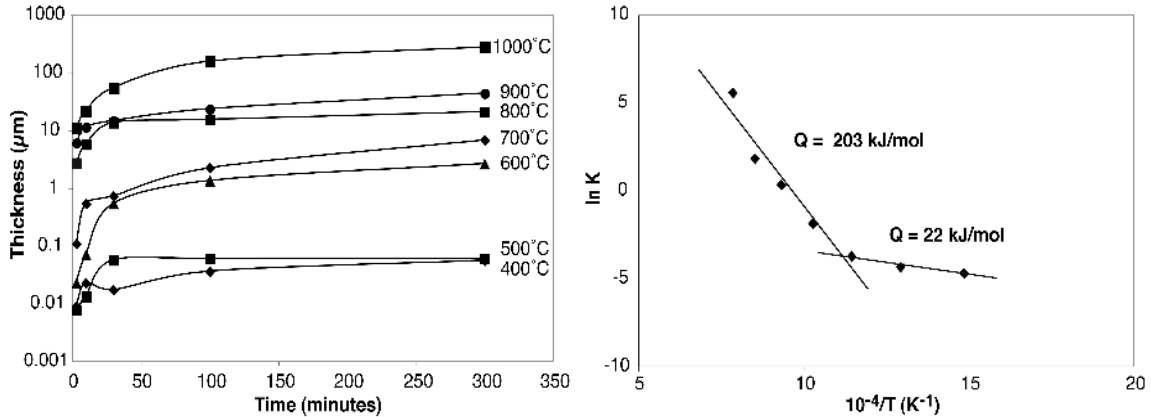

Figure 1: (a) Oxide layer thickness as a function of time and temperature; (b) Arrhenius graph of the temperature-dependent kinetics.

Oxidation Microstructure and Composition

Companion publications document the observed microstructures and composition profiles and relate these microstructures to corrosion behavior and biocompatibility [5,9]. The purpose of this present paper is to discuss high-resolution analyses from microdiffraction and FIB on the 1000°C oxidized samples. Figure 2 shows low-magnification BEI/SEM images from a 300 min oxidized sample. The Ni-rich phases (light) and Ti-rich regions (dark) form lamellar patterns with coarser structures at the outer surface.
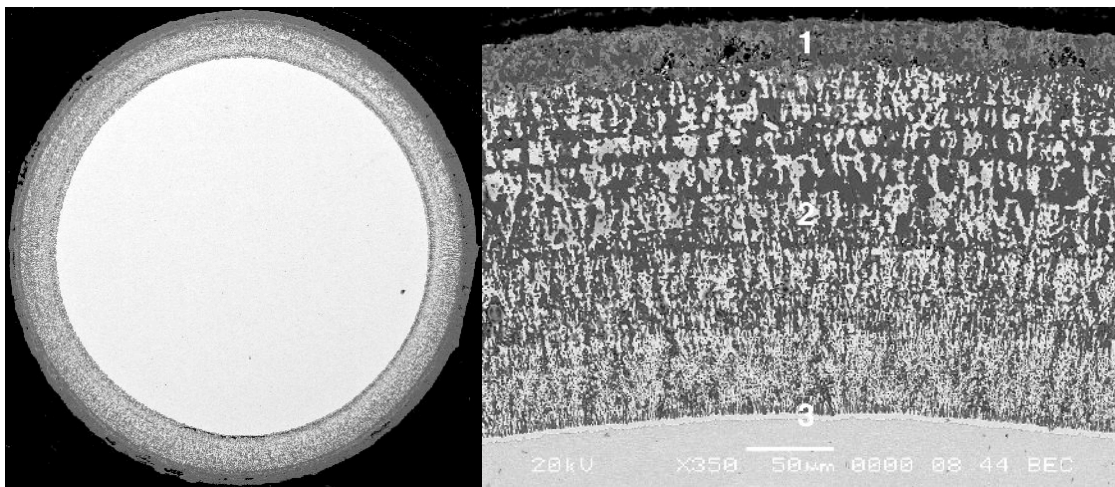

Figure 2: BEI/SEM images of the sample oxidized at 1000°C/300 minutes. The 3mm transverse wire cross section is shown on the left. The three marked regions at the higher magnification (right) are analyzed by synchrotron XRD and FIB in subsequent figures.
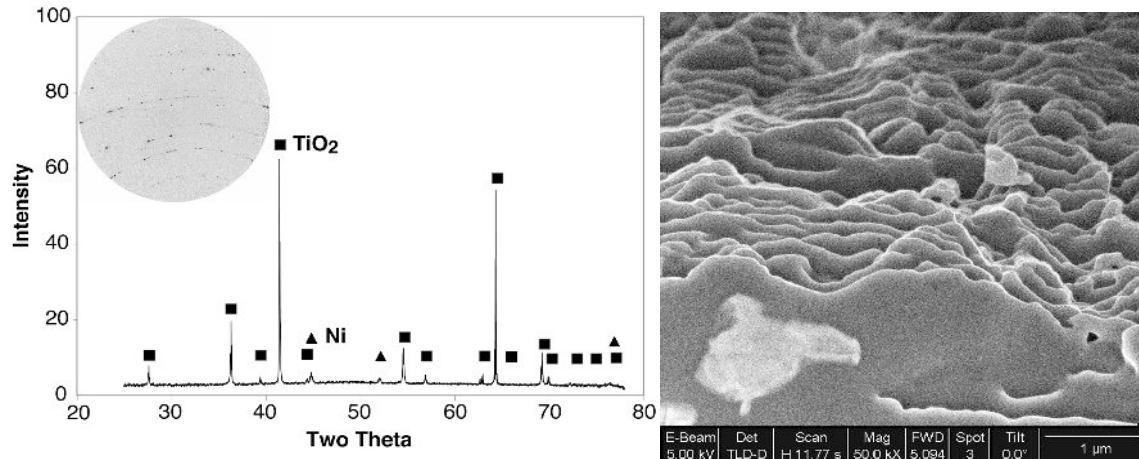
Figure 3: XRD pattern and FIB image of Region 1 shown in Figure 2. The outer layer consists of grey TiO_2 (Rutile) and light Ni. Note the "platelike" surface oxide structure.

Figure 3a is a XRD pattern obtained from Region 1 from the outer surface shown in Figure 2.The powder diffraction pattern was obtained by integrating the intensity over the chi arcs, see inset. The peaks marked with squares are consistent with the structure of TiO_2 in the form of rutile (C4, a = 0.459nm, c = 0.296nm) and the triangles mark the Ni (A1, a = 0.354nm) peaks. The corresponding high-magnification FIB image shows "sheetlike" layers of the outer oxide structure and as well as Ni particles.

Figure 4 is from Region 2 and illustrates the diffraction pattern and FIB image. Both rutile and Ni were observed in this region, as shown in the XRD pattern. The FIB image reveals a unique "3D" structure of the Ni particles that is consistent with 100nm-sized grains inferred from the granularity of the diffraction rings. Since TiNi tends to smear with mechanical polishing, this microstructural feature was only visible after low-energy FIB surface preparation.
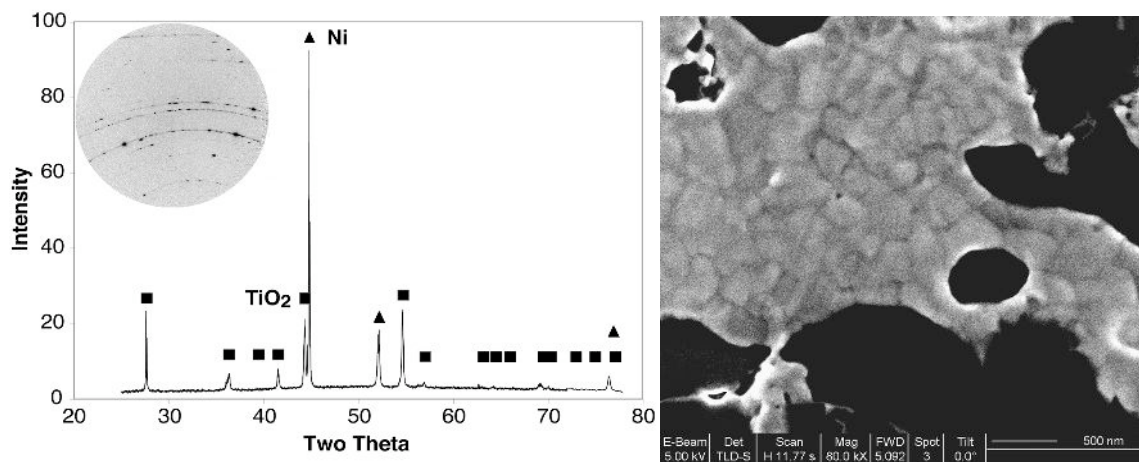

Figure 4: XRD pattern and FIB image of Region 2 shown in Figure 2. The intermediate layer consists of TiO_2 and Ni. Note the nanocrystalline Ni structure.

Figure 5 is from Region 3 and shows the structure and FIB image of the TiNi interface. The XRD pattern reflects the multi-phase regions with TiO_2, Ni, TiNi (diamond symbols, B2, a = 0.30nm), and Ni_3Ti (circles, DO_{24}, a = 0.509nm, c = 0.831nm). Phase identification was verified by chemical composition determined by synchrotron x-ray fluorescence and EDXS from SEM/FIB. The high spatial (~1μm) and angular (0.020° 2θ) resolution of these complementary characterization techniques allowed identification of phases and microstructural features, such as the nanocrystalline Ni grains and interfacial transition from TiNi $\Rightarrow$ Ni_3Ti $\Rightarrow$ Ni, that were not apparent in previous analyses [5,9]. Similarly, earlier investigations of TiNi oxidation used Debye XRD on abraded oxide surfaces [8] or glancing angle XRD [10] and identified NiO and $NiTiO_3$ in addition to TiO_2, Ni, and Ni_3Ti. Ni-rich oxides were not detected in any of the XRD patterns in this study, consistent with XPS data that detect only Ni^0 rather than Ni^{2+}. One possible explanation is that oxide patterns are complex with many similar peaks, which may be difficult to resolve unambiguously with conventional XRD. Furthermore, it is interesting that Ni-rich oxides have only been reported in samples that have been mechanically polished prior to oxidation [8,10,11] rather than electropolishing as in the present investigation.
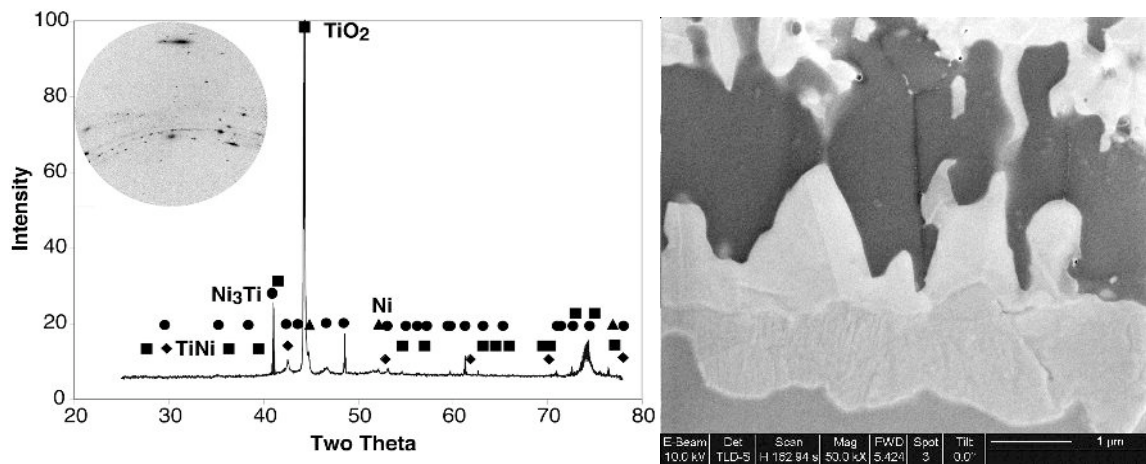

Figure 5: XRD pattern and FIB image of Region 3 shown in Figure 2. The interfacial layer consists of TiO_2 (dark gray), Ni (lightest), Ni_3Ti (light gray) and TiNi (medium gray). Note the fine structure in the Ni_3Ti and Ni and grain boundaries in TiO_2.

The observations from this study as well as earlier work [5,9] are consistent with a model of oxygen absorption on the NiTi surface that reacts with outward diffusing Ti^{4+} to form TiO_2. During the early stages of oxidation, the growth of TiO_2 is the primary contributor to thickness and therefore oxide formation is relatively rapid. However, the preferential oxidation of Ti creates a Ni-rich zone at the $TiNi/TiO_2$ interface. The formation of the Ni_3Ti layer increases the effective diffusion distance with an associated decrease in overall oxidation kinetics. Continued oxide growth therefore involves simultaneous nucleation and growth of TiO_2 and Ni-rich phases. Ultimately, these processes lead to the formation of a thick oxide scale, which easily cracks, exposes Ni to the environment, and leads to poor corrosion and biocompatibility [5]. The phase transformations will be further characterized with transmission electron microscopy and diffraction techniques.

Acknowledgement

References

1. D. Stöckel, A. R. Pelton, and T. Duerig, "Self-expanding Nitinol Stents: Material and Design Considerations, *European Radiology*, 14 (2004), 292-301.

2. C.M. Wayman and T. Duerig, "An Introduction to Martensite and Shape Memory", *Engineering Aspects of Shape Memory Alloys*, ed. T.W. Duerig, *et al.* (London, Butterworth-Heinemann, 1990), 3-20.

3. C. Trépanier, *et al.* "Preliminary Investigation of the Effects of Surface Treatments on Biological Response to Shape Memory NiTi Stents", *J Biomed Mater Res (Appl. Biomater)*, 48 (1999), 165-171.

4. O. Kubaschewski and B.E. Hopkins, *Oxidation of Metals and Alloys*, 2nd ed., (New York, Academic Press, 1962).

5. C. Trépanier, *et al.* "Corrosion Resistance of Oxidized Nitinol", *Proc SMST-2003*, ed. A.R. Pelton and T. Duerig, (Pacific Grove, CA, Inter. Org. SMST, 2004), 367-373.

6. N. Tamura, *et al.*, "Submicron X-Ray Diffraction and its Applications to Problems in Materials and Environmental Science", *Rev Sci Instr,* 73 (2002), 1369-137.

7. C.L. Chu, *et al.*, "Oxidation Behavior of Equiatomic TiNi Alloy in High Temperature Air Environment", *Mater Sci Eng*, A216 (1996), 193-200.

8. V.G. Chuprina, "A Study of the Process of Oxidation of Titanium Nickelide", *Soviet Powder Metallurgy and Metal Ceramics*, 28(4) (1989), 310-314.

9. L. Zhu, J. M. Fino, and A.R. Pelton, "Oxidation of Nitinol", *Proc SMST-2003*, ed. A.R. Pelton and T. Duerig, (Pacific Grove, CA, Inter. Org. SMST, 2004), 357-366.

10. G.S. Firstov, *et al.*, "Surface Oxidation of NiTi Shape Memory Alloy", *Biomaterials*, 22, (2002), 4863-4871

11. C.M. Chan, S. Trigwell, and T. Duerig, "Oxidation of a NiTi Alloy", *Surf and Interf Anal*, 15 (1990), 349-354.